

## Talbot effects induced by gain-loss modulated optical lattices in a coherent atomic medium

Jingliang Feng<sup>1</sup>, Zhaoyang Zhang<sup>2</sup> and Min Xiao<sup>1</sup>

<sup>1</sup>Department of Physics, University of Arkansas, Fayetteville, Arkansas 72701, USA

<sup>2</sup>Key Laboratory for Physical Electronics and Devices of the Ministry of Education & Shaanxi Key Lab of Information Photonic Technique, School of Electronic Science and Engineering, Faculty of Electronic and Information Engineering, Xi'an Jiaotong University, Xi'an 710049, China



(Received 12 February 2021; accepted 8 June 2021; published 21 June 2021)

We investigate the electromagnetically induced Talbot effects resulting from the gain-loss modulated optical lattices constructed in a coherent four-level  $N$ -type atomic system. Both integer and fractional Talbot effects are studied in a parity-time ( $\mathcal{PT}$ ) symmetric optical lattice, quasi- $\mathcal{PT}$ -symmetric optical lattices, and a conventional electromagnetically induced transparency (EIT) optical lattice. Additionally, the visibilities of Talbot images from a  $\mathcal{PT}$ -symmetric optical lattice, quasi- $\mathcal{PT}$ -symmetric optical lattices, and a conventional EIT optical lattice are examined. This study provides insights for understanding the Talbot effects in experiments based on coherent atomic systems with gain and loss properties.

DOI: [10.1103/PhysRevA.103.063516](https://doi.org/10.1103/PhysRevA.103.063516)

### I. INTRODUCTION

The Talbot effect is a near-field diffraction and interference phenomenon, which is also called self-imaging or lensless imaging [1–4]. This effect emerges when a periodic structure is illuminated by a quasimonochromatic coherent light. The original periodic image is replicated at certain imaging planes. These imaging planes are located at even integer multiples of the Talbot distance  $z_T = d^2/\lambda$ , where  $d$  is the spatial period of the pattern and  $\lambda$  is the wavelength of the illuminating light. This effect is called the integer Talbot effect. At a distance  $z = (p/q)z_T$  (here,  $p$  and  $q$  are positive integers,  $p < q$ ), complicated subimage patterns can appear. This property is referred to as the fractional Talbot effect. Nowadays the Talbot effects have already found important applications in optical computing [5], lithography [6], and optical metrology [7]. Recent research on the Talbot effect has further extended to the temporal Talbot effect [8], nonlinear Talbot effect [9,10], quantum Talbot effect [11], angular Talbot effect [12,13], and gain-loss induced Talbot effect [14,15]. These Talbot effects are studied in Bose-Einstein condensates [8], solid materials [9–12,14], and coherent atomic systems [13,15].

Coherent atomic systems provide a fertile platform for observing Talbot effects due to their easy *in situ* reconfigurability and flexible tunability of the parameters [16–18]. The Talbot effect based on an electromagnetically induced grating [19] was theoretically proposed in a three-level ultracold atomic medium [20], which is referred to as an electromagnetically induced Talbot effect (EITE). The integer and fractional EITEs have all been experimentally demonstrated in three-level  $\Lambda$ -type [21] and ladder-type [22] atomic systems, respectively.

Recently, non-Hermitian parity-time ( $\mathcal{PT}$ ) symmetric Hamiltonians have attracted considerable attention since they were first proposed by Bender and Boettcher two decades ago [23]. It was found that this class of Hamiltonians can exhibit entirely real eigenvalue spectra when they satisfy the

$\mathcal{PT}$ -symmetry condition. Many interesting phenomena, such as non-Hermitian optical solitons [24,25], unidirectional invisibility [26–28], non-Hermitian Bloch oscillations [29,30], coherent perfect absorbers [31–33],  $\mathcal{PT}$ -symmetric lasers [34,35], orbital angular momentum lasers [36], and sensing enhancement [37–39] have been discovered in  $\mathcal{PT}$ -symmetric optical configurations. The realizations of  $\mathcal{PT}$ -symmetric potentials in multilevel atomic systems were theoretically proposed [40,41] and an experimental observation of a  $\mathcal{PT}$ -symmetric lattice was demonstrated in a four-level  $N$ -type atomic system [42,43]. With many intriguing phenomena [24–39] observed in  $\mathcal{PT}$ -symmetric optical systems, we envision that it is important to broaden our research on the traditional EITE into the gain-loss modulated, as well as the  $\mathcal{PT}$ -symmetric, coherent atomic systems.

In this article, we investigate the gain-loss modulated Talbot effects in a four-level  $N$ -type atomic configuration. This configuration is driven by a weak signal field and two sets of standing-wave (coupling and pump) laser fields [42]. The induced gain-loss modulated optical lattices inside the atomic vapor are established by the interference of a pair of coupling and pump laser beams, respectively, and an expanded signal field is launched into the dual optical lattices. We study the features of integer and fractional Talbot effects in such a gain-loss modulated optical lattice platform and electromagnetically induced transparency (EIT) optical lattice, in addition to the visibilities of Talbot images from the same optical lattices. This work provides additional insights into the experimental observations of the Talbot effects in the gain-loss modulated optical lattices established in coherent atomic systems.

### II. MODEL

We consider a four-level  $N$ -type atomic system as shown in Fig. 1(a). It consists of two hyperfine states  $F = 2$  (level  $|1\rangle$ ) and  $F = 3$  (level  $|2\rangle$ ) of the ground state  $5S_{1/2}$  and two

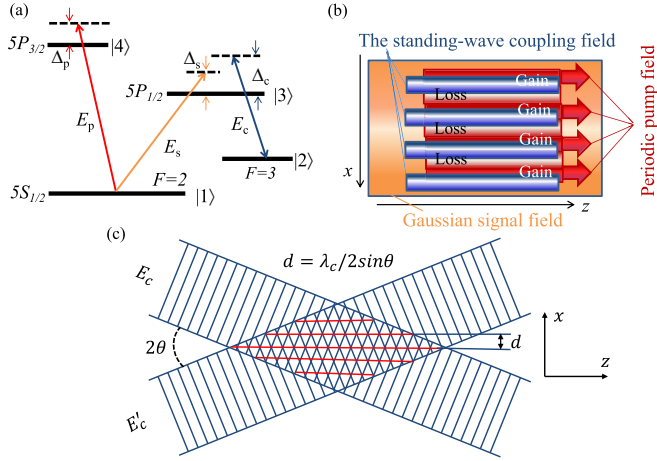


FIG. 1. (a) The energy-level diagram of the four-level  $N$ -type configuration in  $^{85}\text{Rb}$  atomic vapor. (b) The spatial arrangement of the signal, coupling, and pump fields inside the atomic medium. (c) Schematic of the interfering wave fronts of the two coupling beams  $E_c$  and  $E'_c$ .  $x$  and  $z$  represent the transverse and longitudinal directions of propagation, respectively.

excited states  $5P_{1/2}$  (level  $|3\rangle$ ) and  $5P_{3/2}$  (level  $|4\rangle$ ). The signal, coupling, and pump fields drive the atomic transitions  $|1\rangle \leftrightarrow |3\rangle$ ,  $|2\rangle \leftrightarrow |3\rangle$ , and  $|1\rangle \leftrightarrow |4\rangle$ , respectively. The coupling field consists of two laser beams that propagate at an angle  $2\theta$  symmetrically with respect to the  $z$  direction as shown in Fig. 1(c). When they intersect, a standing wave is generated in the rubidium cell along the  $x$  direction with a spatial period  $d = \lambda_c/2 \sin \theta$ , where  $\lambda_c$  is the wavelength of the coupling beam. Similarly, two pump beams, overlapped with the two coupling beams, enter the cell at the same angle  $2\theta$  to form the periodic pump field. The expanded signal beam propagates in the  $z$  direction covering the two sets of optical lattices, as shown in Fig. 1(b).

Under the rotating-wave approximation, the density-matrix equations for the four-level  $N$ -type atomic system are given by [44]

$$\dot{\rho}_{22} = \Gamma_{42}\rho_{44} + \Gamma_{32}\rho_{33} - \Gamma_{21}\rho_{22} + \frac{i}{2}(\rho_{32} - \rho_{23})\Omega_c, \quad (1a)$$

$$\dot{\rho}_{33} = \Gamma_{43}\rho_{44} - \Gamma_{32}\rho_{33} - \Gamma_{31}\rho_{33} + \frac{i}{2}[(\rho_{23} - \rho_{32})\Omega_c + (\rho_{13} - \rho_{31})\Omega_s], \quad (1b)$$

$$\dot{\rho}_{44} = -(\Gamma_{43} + \Gamma_{42} + \Gamma_{41})\rho_{44} + \frac{i}{2}(\rho_{14} - \rho_{41})\Omega_p, \quad (1c)$$

$$\dot{\rho}_{21} = -\tilde{\gamma}_{21}\rho_{21} + \frac{i}{2}(\rho_{31}\Omega_c - \rho_{24}\Omega_p - \rho_{23}\Omega_s), \quad (1d)$$

$$\dot{\rho}_{31} = -\tilde{\gamma}_{31}\rho_{31} + \frac{i}{2}[\rho_{21}\Omega_c - \rho_{34}\Omega_p + (\rho_{11} - \rho_{33})\Omega_s], \quad (1e)$$

$$\dot{\rho}_{41} = -\tilde{\gamma}_{41}\rho_{41} + \frac{i}{2}[-\rho_{43}\Omega_s + (\rho_{11} - \rho_{44})\Omega_p], \quad (1f)$$

$$\dot{\rho}_{32} = -\tilde{\gamma}_{32}\rho_{32} + \frac{i}{2}[\rho_{12}\Omega_s + (\rho_{22} - \rho_{33})\Omega_c], \quad (1g)$$

$$\dot{\rho}_{42} = -\tilde{\gamma}_{42}\rho_{42} + \frac{i}{2}(\rho_{12}\Omega_p - \rho_{43}\Omega_c), \quad (1h)$$

$$\dot{\rho}_{43} = -\tilde{\gamma}_{43}\rho_{43} + \frac{i}{2}(\rho_{13}\Omega_p - \rho_{42}\Omega_c - \rho_{41}\Omega_s), \quad (1i)$$

where  $\Omega_s = \mu_{13}E_s/\hbar$ ,  $\Omega_c = \mu_{23}E_c/\hbar$ , and  $\Omega_p = \mu_{14}E_p/\hbar$  are the Rabi frequencies corresponding to the signal, coupling, and pump fields, respectively, and  $\mu_{ij}$  is the dipole moment between levels  $|i\rangle$  and  $|j\rangle$ .  $\Gamma_{ij}$  is the decay rate between levels  $|i\rangle$  and  $|j\rangle$ , and  $\gamma_{ij} = (\Gamma_i + \Gamma_j)/2$  is the decoherence rate.  $\tilde{\gamma}_{21} = \gamma_{21} - i(\Delta_s - \Delta_c)$ ,  $\tilde{\gamma}_{31} = \gamma_{31} - i\Delta_s$ ,  $\tilde{\gamma}_{41} = \gamma_{41} - i\Delta_p$ ,  $\tilde{\gamma}_{32} = \gamma_{32} - i\Delta_c$ ,  $\tilde{\gamma}_{42} = \gamma_{42} - i(\Delta_c + \Delta_p - \Delta_s)$ ,  $\tilde{\gamma}_{43} = \gamma_{43} - i(\Delta_p - \Delta_s)$ .  $\Delta_s = \omega_s - \omega_{31}$ ,  $\Delta_c = \omega_c - \omega_{32}$ , and  $\Delta_p = \omega_p - \omega_{41}$  are the frequency detunings of the signal, coupling, and pump fields, respectively. The susceptibility of the atomic medium can be obtained through the expression  $\chi = \frac{2N\mu_{13}}{\epsilon_0 E_s} \rho_{31}$ . Given that  $n = \sqrt{1 + \chi} \approx 1 + \chi/2$ ,  $\chi = \chi' + i\chi''$ , and  $n = n_0 + n_R + n_I$ , the real and imaginary parts of the refractive index can be written as  $n_R \approx \frac{1}{2}\chi' = \frac{N\mu_{13}}{\epsilon_0 E_s} \text{Re}(\rho_{31})$  and  $n_I \approx \frac{1}{2}\chi'' = \frac{N\mu_{13}}{\epsilon_0 E_s} \text{Im}(\rho_{31})$ . Here,  $n_0 = 1$  is the background index of the atomic medium.

### III. CONSTRUCTIONS OF A $\mathcal{PT}$ -SYMMETRIC OPTICAL LATTICE AND A CONVENTIONAL EIT OPTICAL LATTICE

We begin by considering the realization of a  $\mathcal{PT}$ -symmetric optical lattice. By solving the coupled equations in Eq. (1) numerically under properly chosen parameters, one can obtain the real (dispersion) and imaginary (gain or absorption) parts of the susceptibility versus the transverse position  $x$  as shown in Figs. 2(a) and 2(b) [40,42]. The fact that the real and imaginary parts of the susceptibility are even and odd functions with respect to the position  $x$  and the relationship of  $n_R \approx \frac{1}{2}\chi'$  and  $n_I \approx \frac{1}{2}\chi''$  indicates that the condition  $n(x) = n^*(-x)$  is approximately satisfied, meaning that the  $\mathcal{PT}$ -symmetric structure with alternating gain and loss waveguides can be established in such an atomic configuration. To achieve the exact  $\mathcal{PT}$ -symmetric condition in the current scheme, the values of the real part of the susceptibility versus  $\Delta_s$  at  $\Omega_p = 0$  and  $\Omega_p \neq 0$  must be the same, while the corresponding imaginary parts must have the same absolute value but opposite signs. In our calculation, we only found one signal frequency detuning  $\Delta_s = -2\pi \times 15.05$  MHz which can make this condition satisfied. Thus, this  $\mathcal{PT}$ -symmetry condition cannot be easily obtained without specially selected parameters.

When the pump beams are absent, the atomic system becomes a traditional three-level  $\Lambda$ -type EIT configuration [45,46]. The induced optical lattice established by the interference of the pair of coupling beams is referred to as a conventional EIT optical lattice. The numerically calculated real and imaginary parts of the susceptibility versus the transverse position  $x$  under specially chosen parameters are shown in Figs. 3(a) and 3(b). One can see that both of them are even functions of  $x$ . There is no Raman gain in this simple configuration because the imaginary part of the susceptibility is always greater than 0.

### IV. TALBOT EFFECTS INDUCED IN A $\mathcal{PT}$ -SYMMETRIC OPTICAL LATTICE AND A CONVENTIONAL EIT OPTICAL LATTICE

The propagation dynamics of the signal field within the cell obeys the Maxwell's equation, and its transmission at the

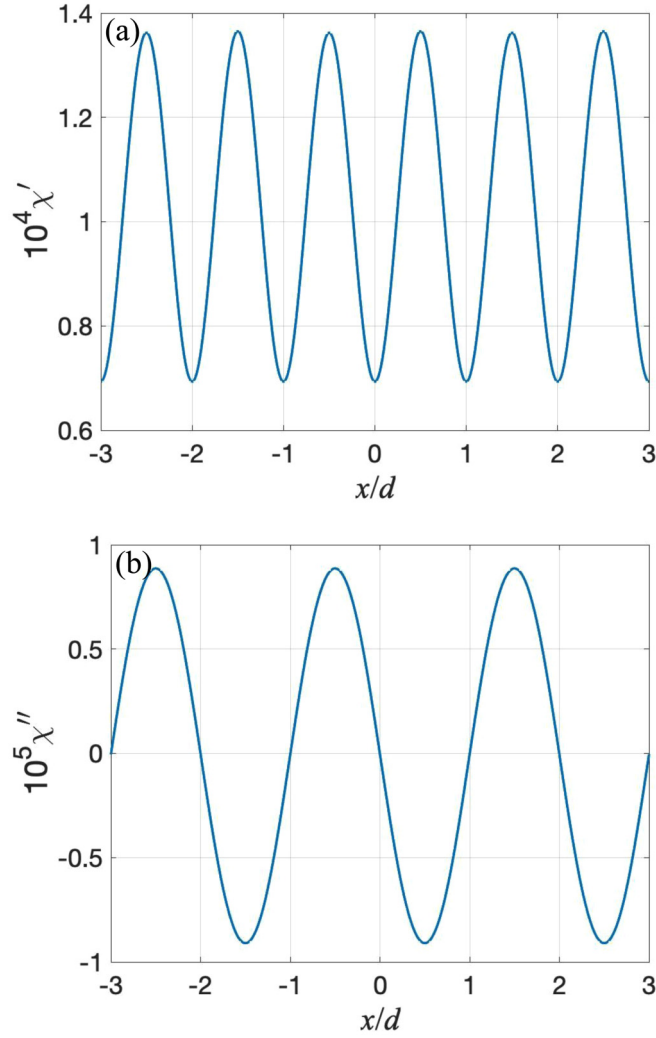


FIG. 2. (a) Real and (b) imaginary parts of the susceptibility for a signal field as a function of position  $x$  with the coupling and pump intensities spatially modified.  $N = 10^{13} \text{ cm}^{-3}$ ,  $\Omega_s = 2\pi \times 10 \text{ MHz}$ ,  $\Omega_c = 2\pi \times 0.2[1 + \cos(\pi x/d)] \text{ MHz}$ ,  $\Omega_p = 2\pi \times 6 \text{ MHz}$  in the gain region and  $\Omega_p = 0$  in the loss region,  $\Delta_p = 40 \text{ MHz}$ ,  $\Delta_c = -100 \text{ MHz}$ , and  $\Delta_s = -2\pi \times 15.05 \text{ MHz}$ .  $d$  is the periodicity of the coupling and pump fields.

output surface is

$$E_s(x, L) = E_s(x, 0) \exp(-k_s \chi'' L/2) \exp(ik_s \chi' L/2), \quad (2)$$

where  $\chi'$  and  $\chi''$  are the real and imaginary parts of the susceptibility  $\chi$ , respectively,  $k_s = 2\pi/\lambda_s$ ,  $E_s(x, 0)$  is the input signal profile, and  $L$  is the length of the cell.

Using the Fresnel-Kirchhoff diffraction integral, the output signal field  $E_s$  at a distance  $z$  from the output surface of the medium is proportional to [47]

$$E_s(X, z) \propto \int_{-\infty}^{\infty} E_s(x, L) \exp\left[ik_s \left(z + \frac{x^2}{2z} - \frac{xX}{z} + \frac{X^2}{2z}\right)\right] dx, \quad (3)$$

where  $x$  and  $X$  are the coordinates in the object and observation planes, respectively. Because of the periodicity of  $\chi$  in

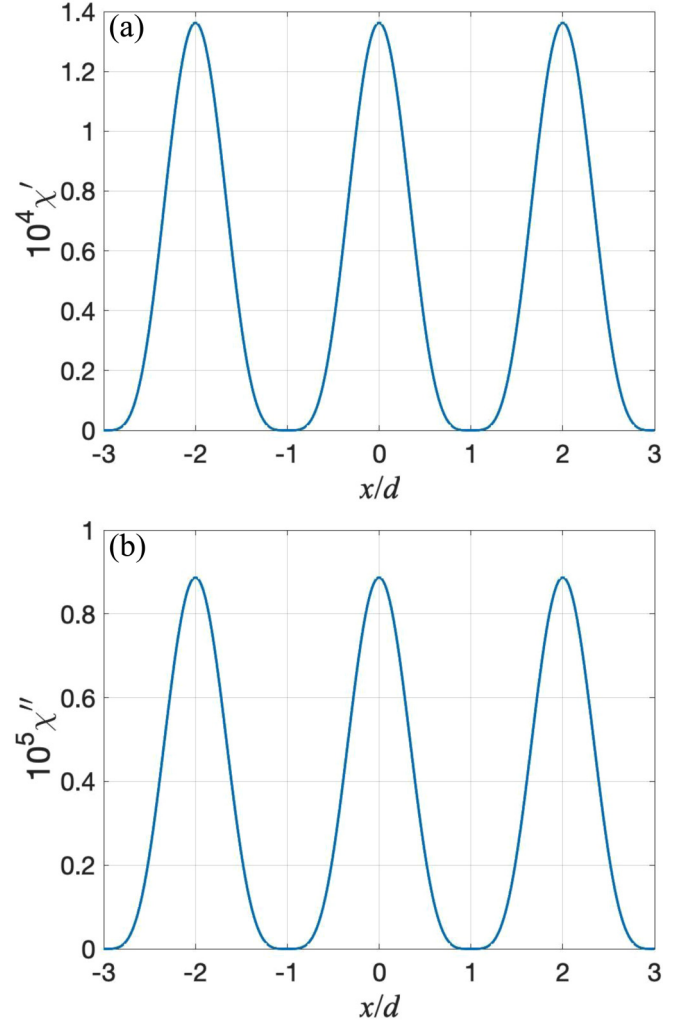


FIG. 3. (a) Real and (b) imaginary parts of the susceptibility for a signal field as a function of position  $x$  with only the spatially modulated coupling field turned on to connect a three-level system. Relevant parameters are the same as in Fig. 2 except  $\Omega_p = 0$ .  $d$  is the periodicity of the coupling field.

Figs. 2 and 3,  $E_s(x, L)$  can be recast into a Fourier series,

$$E_s(x, L) = \sum_{n=-\infty}^{+\infty} C_n \exp(i2\pi nx/d), \quad (4)$$

where  $C_n = \frac{1}{d} \int_0^d e^{-k_s \chi'' L/2} e^{ik_s \chi' L/2} e^{-i2\pi nx/d} dx$  is the coefficient of the  $n$ th harmonic field. By substituting Eq. (4) into Eq. (3) and completing the integral, we can obtain the traditional Talbot effect described by [47]

$$E_s(X, z) \propto \sum_{n=-\infty}^{+\infty} C_n \exp(-i\pi n^2 z/z_T) \exp(i2\pi nX/d), \quad (5)$$

where  $z_T = d^2/\lambda_s$  is the Talbot length,  $d$  is the spatial period along the transverse direction, and  $\lambda_s$  is the wavelength of the signal field.

According to Eq. (5), the signal transmission with a distance of  $mz_T$  can repeat the field amplitude at the output plane of the cell with and without a shifted half period  $d/2$

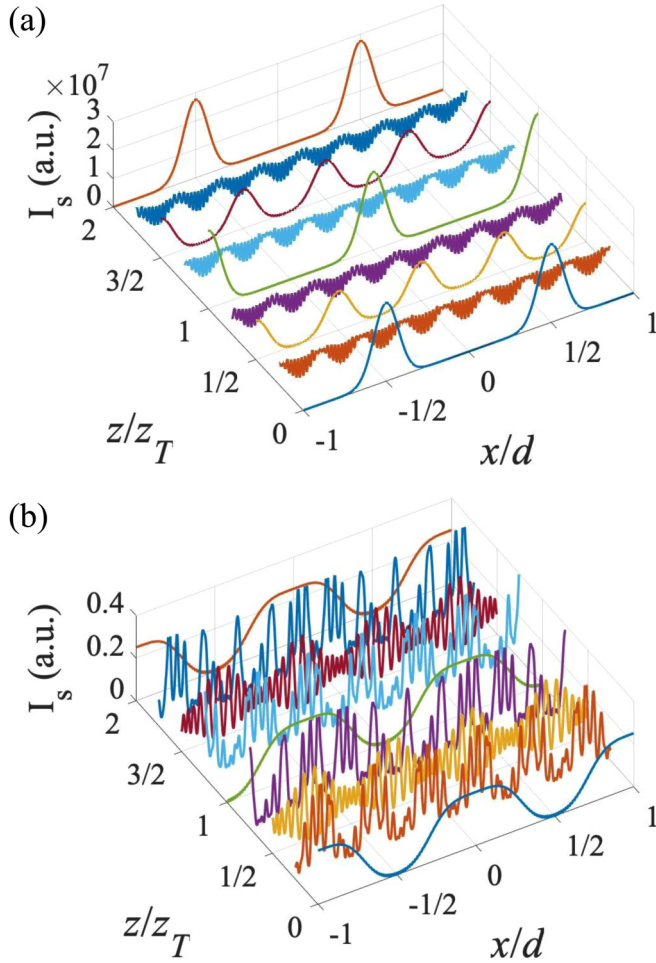


FIG. 4. Normalized intensity distributions of the diffracted signal field at various propagation distances within two spatial periods under (a) the four-level  $N$ -type configuration and (b) the three-level EIT configuration at  $z = 0, z = z_T/4, z = z_T/2, z = 3z_T/4, z = z_T, z = 5z_T/4, z = 3z_T/2, z = 7z_T/4, z = 2z_T$ .  $\lambda_s = 794.97$  nm,  $k_s = 2\pi/\lambda_s$ , and  $d = 114$   $\mu\text{m}$ .  $L = 2.5$  is given in the units of  $k_s d^2$ . The optical detunings used are the same as the ones in Fig. 2.

for odd and even integers  $m$ , respectively. Moreover, the fractional Talbot images appear at all rational multiples of  $z_T$ , i.e.,  $z = (p/q)z_T$ , where  $p, q$  are positive integers,  $p < q$ .

Figures 4(a) and 4(b) give typical transverse profiles of the normalized intensity of the diffracted signal wave under the four-level  $N$ -type configuration and the three-level EIT configuration at distances  $z = (p/4)z_T$  ( $p = 0, 1, 2, \dots, 8$ ) from the output surface of the medium. Figure 4(a) shows that the intensity of the diffracted wave can be substantially larger (i.e.,  $10^7$ ) than the intensity of the input signal beam. This intensity increase is caused by the gain channels in the  $\mathcal{PT}$ -symmetric optical lattice. For fractional Talbot planes, the field amplitude and periodicity of the image undergo significant changes. The diffraction pattern is periodic but its intensity no longer replicates the amplitude at the output of the cell. The transverse profile at each fractional Talbot distance displays a distinct pattern and the period of the fractional Talbot image is always smaller than that of the integer Talbot image pattern. One can also see that the maximum intensity

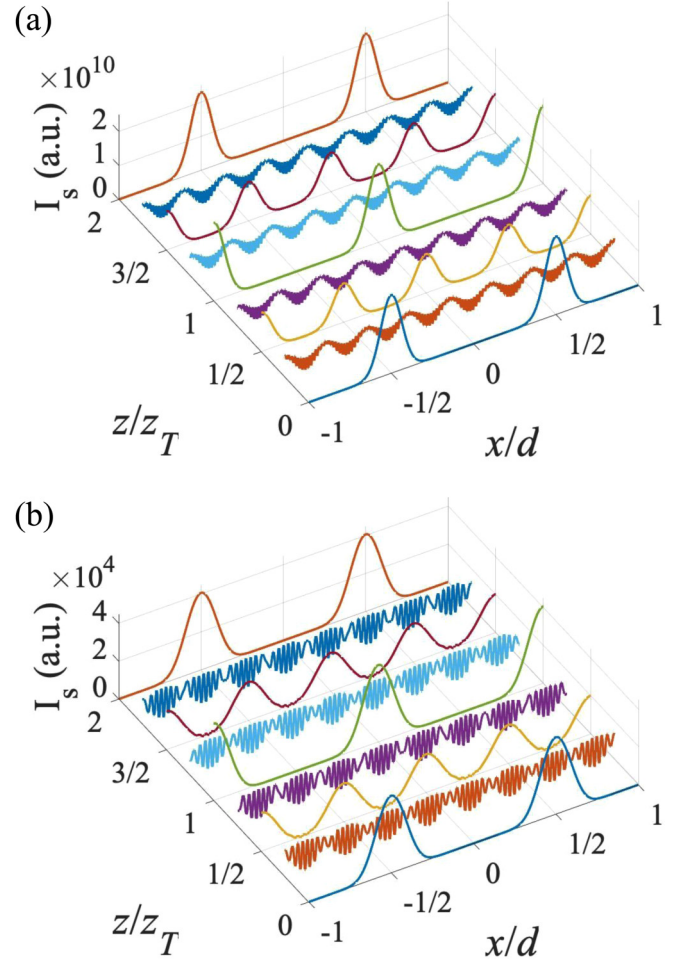


FIG. 5. Normalized intensity distributions of the diffracted signal field at various propagation distances within two spatial periods under the four-level  $N$ -type configuration.  $z = 0, z = z_T/4, z = z_T/2, z = 3z_T/4, z = z_T, z = 5z_T/4, z = 3z_T/2, z = 7z_T/4, z = 2z_T$  when (a) gain/loss = 3.17 and (b) gain/loss = 0.22, respectively. Other parameters are the same as in Fig. 4.

of the fractional Talbot images is always smaller than that of the integer Talbot images under this  $\mathcal{PT}$ -symmetric condition. From Fig. 4(b) we can see the intensity of the diffracted signal wave is decreased due to residue absorption of the medium under the three-level EIT configuration. In this case, the fractional Talbot images are noisier, mainly due to the lack of gain channels in the EIT optical lattice which reduces the visibility of the Talbot images (see more discussions below). In addition, the periods for the fractional Talbot images are smaller as compared to the period for the integer Talbot images, which is consistent with the experimental observation reported previously [21,22].

As mentioned before, the  $\mathcal{PT}$ -symmetry condition, that is, balanced gain and loss (gain/loss = 1), is not a common scenario. To complement, we have studied the Talbot effects for unbalanced gain and loss cases (gain/loss  $\neq 1$ ), namely, quasi- $\mathcal{PT}$ -symmetric cases [48,49]. Figures 5(a) and 5(b) exhibit the transverse profiles of normalized intensity of the diffracted signal wave under the four-level  $N$ -type configuration at distances  $z = (p/4)z_T$  ( $p = 0, 1, 2, \dots, 8$ ) from the

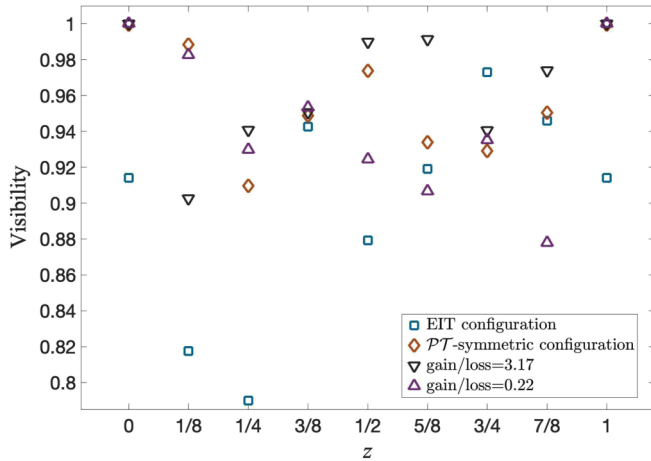


FIG. 6. Visibility comparisons of the Talbot images for the conventional EIT optical lattice,  $\mathcal{PT}$ -symmetric optical lattice, and quasi- $\mathcal{PT}$ -symmetric optical lattices (for gain/loss = 3.17 and gain/loss = 0.22, respectively) as a function of propagation distance within one Talbot length.

output surface of the medium when gain/loss = 3.17 and gain/loss = 0.22, respectively. In our numerical simulations, we only allow the frequency detuning of the signal field to change such that the ratio of gain to loss varies along with the changing frequency detuning of the signal field. The value of gain/loss = 3.17 can be obtained when the signal frequency detuning is set to  $\Delta_s = -2\pi \times 15.25$  MHz, and gain/loss = 0.22 can be obtained at  $\Delta_s = -2\pi \times 14.80$  MHz. In Figs. 5(a) and 5(b), one can see that the intensity of the diffracted signal wave increases for both cases, i.e., gain/loss = 3.17 and gain/loss = 0.22, and when gain/loss = 3.17, the intensity increases more. This indicates that a larger gain can give rise to a greater intensity. On the other hand, the periods of the fractional Talbot images are always smaller than that of the integer Talbot images, and distinct image patterns occur at the same fractional Talbot distances under the two conditions (i.e., gain/loss > 1 and gain/loss < 1).

From Figs. 4 and 5, one can see that the Talbot lengths for the  $\mathcal{PT}$ -symmetric optical lattice, conventional EIT optical lattice, and quasi- $\mathcal{PT}$ -symmetric optical lattices (gain and loss are not balanced) are the same, in line with the result reported in Ref. [50]. There is a half-period shift with respect to the output profile of the signal field at the first Talbot length for all cases. This is in agreement with the prediction from Eq. (5). The periods of the fractional Talbot images at distances  $z = \frac{1}{2}z_T$  and  $z = \frac{3}{2}z_T$  are the same, to be half the period of the integer Talbot images for all the optical lattices, supported by the theoretical calculation.

The intensity visibilities, defined as  $\text{visibility} = (I_{\max} - I_{\min}) / (I_{\max} + I_{\min})$ , of the fractional Talbot images are likely to provide additional information about the coherent atomic medium; thus, we examined the intensity visibilities for the

conventional EIT optical lattice,  $\mathcal{PT}$ -symmetric optical lattice, and quasi- $\mathcal{PT}$ -symmetric optical lattices (gain/loss = 3.17 and gain/loss = 0.22, respectively) as shown in Fig. 6. It is clear that the intensity contrast (visibility) for the  $\mathcal{PT}$ -symmetric optical lattice and quasi- $\mathcal{PT}$ -symmetric optical lattices is higher than that for the conventional EIT optical lattice at most of the propagation distances. When the ratio of gain to loss is greater, the visibility would be better at most of the propagation distances. For this reason, we can obtain an improvement of the intensity contrast of the Talbot images by employing a medium with gain. In other words, the introduction of the gain which exists in the four-level  $N$ -type atomic system would make it easier to observe the fractional Talbot images. Collectively, our scheme offers a nondestructive way to image ultracold atomic gas samples [20]. In this study, the signal refers to the intensity of the bright fringe, that is,  $I_{\max}$  in the definition of visibility, and the noise denotes the intensity at the dark fringe, i.e.,  $I_{\min}$  in the definition of visibility. The signal-to-noise ratio of the Talbot images can increase by improving the visibility and contrast of the Talbot images, therefore allowing more accurate information about the density distribution and other coherent properties of the ultracold atomic gas samples.

## V. SUMMARY

We have investigated the integer and fractional Talbot effects induced in a  $\mathcal{PT}$ -symmetric optical lattice, conventional EIT optical lattice, and quasi- $\mathcal{PT}$ -symmetric optical lattices. The intensity of the diffracted signal wave from the  $\mathcal{PT}$ -symmetric optical lattice and quasi- $\mathcal{PT}$ -symmetric optical lattices can be substantially increased due to the gain channels in the optical lattices, while for the conventional EIT optical lattice, the intensity of the diffracted wave is decreased because of the absorption in the optical lattice. The visibilities of the fractional Talbot images from the  $\mathcal{PT}$ -symmetric optical lattice and quasi- $\mathcal{PT}$ -symmetric optical lattices are larger than that from the conventional EIT optical lattice for most of the propagation distances. This increase of visibility can be explained by the gain that exists in the four-level  $N$ -type atomic system. Compared to the scheme used in Ref. [50], we would like to emphasize that there is no intrinsic restriction for the signal beam size in our proposed scheme. Considering the inhomogeneous distribution of the atomic gas samples, we believe that a proper beam size is essential for practical experiments since more accurate information on atomic distribution would be obtained via the output signal patterns when more of the atomic cloud is covered by the signal beam. Any beam size that is required to cover the entire atomic cloud should be suitable for the current scheme. Considering the large Kerr nonlinearity [51] that exists in this system, this research can be extended to further study the features of the  $\mathcal{PT}$ -symmetric nonlinear Talbot effects.

[1] H. F. Talbot, *Philos. Mag.* **9**, 401 (1836).  
 [2] L. Rayleigh, *Philos. Mag.* **11**, 196 (1881).

[3] K. Patorski, in *Progress in Optics*, edited by E. Wolf (North-Holland, Amsterdam, 1989), Vol. 27, p. 1108.

- [4] J. Wen, Y. Zhang, and M. Xiao, *Adv. Opt. Photon.* **5**, 83 (2013).
- [5] K. Patorski, *Prog. Opt.* **27**, 1 (1989).
- [6] Q. Wu, H. Xia, H. Jia, H. Wang, C. Jiang, L. Wang, J. Zhao, R. Tai, S. Xiao, D. Zhang, S. Yang, and J. Jiang, *Opt. Lett.* **44**, 1031 (2019).
- [7] L. M. Sanchez-Brea, F. J. Torcal-Milla, and E. Bernabeu, *Opt. Commun.* **278**, 23 (2007).
- [8] L. Deng, E. W. Hagley, J. Denschlag, J. E. Simsarian, M. Edwards, C. W. Clark, K. Helmerson, S. L. Rolston, and W. D. Phillips, *Phys. Rev. Lett.* **83**, 5407 (1999).
- [9] Y. Zhang, J. Wen, S. N. Zhu, and M. Xiao, *Phys. Rev. Lett.* **104**, 183901 (2010).
- [10] J. Wen, Y. Zhang, S. N. Zhu, and M. Xiao, *J. Opt. Soc. Am. B* **28**, 275 (2011).
- [11] X. B. Song, H. B. Wang, J. Xiong, K. Wang, X. Zhang, K. H. Luo, and L. A. Wu, *Phys. Rev. Lett.* **107**, 033902 (2011).
- [12] J. Azaña and H. Guillet de Chatellus, *Phys. Rev. Lett.* **112**, 213902 (2014).
- [13] T. Qiu and G. Yang, *J. Phys. B* **48**, 245502 (2015).
- [14] H. Ramezani, D. N. Christodoulides, V. Kovanis, I. Vitebskiy, and T. Kottos, *Phys. Rev. Lett.* **109**, 033902 (2012).
- [15] V. G. Arkhipkin and S. A. Myslivets, *Phys. Rev. A* **100**, 063835 (2019).
- [16] Z. Zhang, F. Li, G. Malpuech, Y. Zhang, O. Bleu, S. Koniakhin, C. Li, Y. Zhang, Y. Zhang, M. Xiao, and D. D. Solnyshkov, *Phys. Rev. Lett.* **122**, 233905 (2019).
- [17] Z. Zhang, R. Wang, Y. Zhang, Y. V. Kartashov, F. Li, H. Zhong, H. Guan, K. Gao, F. Li, Y. Zhang, and M. Xiao, *Nat. Commun.* **11**, 1902 (2020).
- [18] Z. Zhang, S. Liang, F. Li, S. Ning, Y. Li, G. Malpuech, Y. Zhang, M. Xiao, and D. Solnyshkov, *Optica* **7**, 455 (2020).
- [19] H. Y. Ling, Y.-Q. Li, and M. Xiao, *Phys. Rev. A* **57**, 1338 (1998).
- [20] J. Wen, S. Du, H. Chen, and M. Xiao, *Appl. Phys. Lett.* **98**, 081108 (2011).
- [21] Z. Zhang, X. Liu, D. Zhang, J. Sheng, Y. Zhang, Y. Zhang, and M. Xiao, *Phys. Rev. A* **97**, 013603 (2018).
- [22] J. Yuan, C. Wu, Y. Li, L. Wang, Y. Zhang, L. Xiao, and S. Jia, *Opt. Express* **27**, 92 (2019).
- [23] C. M. Bender and S. Boettcher, *Phys. Rev. Lett.* **80**, 5243 (1998).
- [24] Z. H. Musslimani, K. G. Makris, R. El-Ganainy, and D. N. Christodoulides, *Phys. Rev. Lett.* **100**, 030402 (2008).
- [25] M. Wimmer, A. Regensburger, M.-A. Miri, C. Bersch, D. N. Christodoulides, and U. Peschel, *Nat. Commun.* **6**, 7782 (2015).
- [26] Z. Lin, H. Ramezani, T. Eichelkraut, T. Kottos, H. Cao, and D. N. Christodoulides, *Phys. Rev. Lett.* **106**, 213901 (2011).
- [27] B. Peng, S. K. Özdemir, F. Lei, F. Monifi, M. Gianfreda, G. L. Long, S. Fan, F. Nori, C. M. Bender, and L. Yang, *Nat. Phys.* **10**, 394 (2014).
- [28] L. Feng, Y.-L. Xu, W. S. Fegadolli, M.-H. Lu, J. E. B. Oliveira, V. R. Almeida, Y.-F. Chen, and A. Scherer, *Nat. Mater.* **12**, 108 (2013).
- [29] S. Longhi, *Phys. Rev. Lett.* **103**, 123601 (2009).
- [30] M. Wimmer, M. A. Miri, D. N. Christodoulides, and U. Peschel, *Sci. Rep.* **5**, 17760 (2015).
- [31] S. Longhi, *Phys. Rev. A* **82**, 031801(R) (2010).
- [32] S. Longhi and L. Feng, *Opt. Lett.* **39**, 5026 (2014).
- [33] Y. D. Chong, L. Ge, H. Cao, and A. D. Stone, *Phys. Rev. Lett.* **105**, 053901 (2010).
- [34] H. Hodaei, M. A. Miri, M. Heinrich, D. N. Christodoulides, and M. Khajavikhan, *Science* **346**, 975 (2014).
- [35] L. Feng, Z. J. Wong, R.-M. Ma, Y. Wang, and X. Zhang, *Science* **346**, 972 (2014).
- [36] P. Miao, Z. Zhang, J. Sun, W. Walasik, S. Longhi, N. M. Litchinitser, and L. Feng, *Science* **353**, 464 (2016).
- [37] J. Wiersig, *Phys. Rev. Lett.* **112**, 203901 (2014).
- [38] W. Chen, S. K. Özdemir, G. Zhao, J. Wiersig, and L. Yang, *Nature (London)* **548**, 192 (2017).
- [39] H. Hodaei, A. U. Hassan, S. Wittek, H. Garcia-Gracia, R. El-Ganainy, D. N. Christodoulides, and M. Khajavikhan, *Nature (London)* **548**, 187 (2017).
- [40] J. Sheng, M. A. Miri, D. N. Christodoulides, and M. Xiao, *Phys. Rev. A* **88**, 041803(R) (2013).
- [41] C. Hang, G. Huang, and V. V. Konotop, *Phys. Rev. Lett.* **110**, 083604 (2013).
- [42] Z. Zhang, Y. Zhang, J. Sheng, L. Yang, M.-A. Miri, D. N. Christodoulides, B. He, Y. Zhang, and M. Xiao, *Phys. Rev. Lett.* **117**, 123601 (2016).
- [43] Z. Zhang, L. Yang, J. Feng, J. Sheng, Y. Zhang, Y. Zhang, and M. Xiao, *Laser Photon. Rev.* **12**, 1800155 (2018).
- [44] M. O. Scully and M. S. Zubairy, *Quantum Optics* (Cambridge University Press, Cambridge, UK, 1997).
- [45] S. E. Harris, *Phys. Today* **50**(7), 36 (1997).
- [46] J. Gea-Banacloche, Y. Q. Li, S. Z. Jin, and M. Xiao, *Phys. Rev. A* **51**, 576 (1995).
- [47] M. Born and E. Wolf, *Principles of Optics: Electromagnetic Theory of Propagation, Interference and Diffraction of Light* (Elsevier, Amsterdam, 2013).
- [48] O. Marco and S. Alexander, *J. Opt.* **16**, 065501 (2014).
- [49] A. Lupu, H. Benisty, and A. Degiron, *Opt. Express* **21**, 21651 (2013).
- [50] C. Hang, W. Li, and G. Huang, *Phys. Rev. A* **100**, 043807 (2019).
- [51] H. Kang and Y. Zhu, *Phys. Rev. Lett.* **91**, 093601 (2003).